Enhanced efficiency and stability of polymer solar cells using solution-processed nickel oxide as hole transport material

Parthiban, Shanmugam; Kim, Seungmin; Tamilavan, Vellaiappillai; Lee, Jihoon; Shin, Insoo; Dhayalan, Yuvaraj; Jung, Yun Kyung; Hyun, Myung Ho; Jeong, Jung Hyun; Park, Sung Heum

DOI:
10.1016/j.cap.2017.06.002

Document Version
Peer reviewed version

Citation for published version (Harvard):
Parthiban, S, Kim, S, Tamilavan, V, Lee, J, Shin, I, Dhayalan, Y, Jung, YK, Hyun, MH, Jeong, JH & Park, SH 2017, 'Enhanced efficiency and stability of polymer solar cells using solution-processed nickel oxide as hole transport material', Current Applied Physics, vol. 17, no. 10, pp. 1232-1237.
https://doi.org/10.1016/j.cap.2017.06.002

Accepted Manuscript

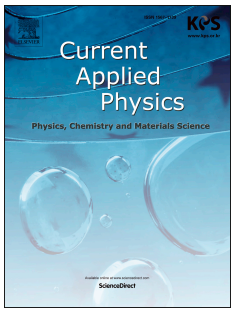

Enhanced efficiency and stability of polymer solar cells using solution-processed nickel oxide as hole transport material

Shanmugam Parthiban, Seungmin Kim, Vellaiappillai Tamilavan, Jihoon Lee, Insoo Shin, D. Yuvaraj, Yun Kyung Jung, Myung Ho Hyun, Jung Hyun Jeong, Sung Heum Park

PII: S1567-1739(17)30178-5

DOI: 10.1016/j.cap.2017.06.002

Reference: CAP 4525

To appear in: *Current Applied Physics*

Received Date: 26 January 2017

Revised Date: 8 May 2017

Accepted Date: 7 June 2017

Please cite this article as: S. Parthiban, S. Kim, V. Tamilavan, J. Lee, I. Shin, D. Yuvaraj, Y.K. Jung, M.H. Hyun, J.H. Jeong, S.H. Park, Enhanced efficiency and stability of polymer solar cells using solution-processed nickel oxide as hole transport material, *Current Applied Physics* (2017), doi: 10.1016/j.cap.2017.06.002.

Enhanced Efficiency and Stability of Polymer Solar Cells using Solution-processed Nickel Oxide as Hole Transport Material

Shanmugam Parthiban[a+], Seungmin Kim[a+], Vellaiappillai Tamilavan[a], Jihoon Lee[a], Insoo Shin[a], D.Yuvaraj[b], Yun Kyung Jung[c], Myung Ho Hyun[d], Jung Hyun Jeong[a], and Sung Heum Park[a,*]

[a] Department of Physics, Pukyong National University, Busan 608-737, Republic of Korea
[b] School of Electronic, Electrical and System Engineering, University of Birmingham, Birmingham, B15 2TT, United Kingdom
[c] School of Biomedical Engineering, Inje University, Inje-ro 197, Gimhae, Gyeongnam 50834, Republic of Korea
[d] Department of Chemistry, Chemistry Institute for Functional Materials, Pusan National University, Busan 690-735, Republic of Korea.

[+] These authors made equal contribution to this work.

Abstract

Solution-processed nickel oxide (s-NiO_x) was synthesized for use as hole-transport layers (HTLs) in the fabrication of polymer solar cell (PSC) devices. The s-NiO_x thin-films were deposited using spin-coating and post-annealed at 300 °C, 400 °C, or 500 °C. With increased annealing temperature, the nickel acetate precursor decomposes more fully and forms s-NiO_x films that show larger crystalline grain sizes with lower root mean square surface roughness. Bulk heterojunction solar cells fabricated with the new random polymer RP(BDT-PDBT) and [6,6]-phenyl-C_{70}-butyric acid methyl ester ($PC_{70}BM$) using s-NiO_x as HTLs exhibit a 4.46% enhancement in power conversion efficiency and better stability compared to conventional PSCs using poly (3,4-ethylenedioxythiophene):poly(styrene sulfonate) as HTLs. We believe that the solution-processable and highly stable s-NiO_x could be a potential alternative for functional interface materials in optoelectronic devices.

Bulk heterojunction polymer solar cells (BHJ PSCs) offer a promising alternative in the development of low-cost, low-temperature-processed, and roll-to-roll-fabricated larger-area solar cells [1-5]. The power conversion efficiency (PCE) of BHJ PSCs has steadily improved, approaching 11%, by using various polymers [6-8], metal oxide layers [9-11], and new device structures [12-14] in recent years. Traditional BHJ PSCs contain transparent conducting oxide (TCO) anodes, hole transport layers (HTLs), photoactive layers, electron transport layers, and a top cathode. In particular, the use of an efficient HTL with high optical transparency, good chemical stability, and good electron-blocking ability between the TCO and photoactive layer facilitates better hole transport, consequently improving device performance [15-18]. In typical PSCs, poly(3,4-ethylenedioxy-thiophene):poly(styrene sulfonate) (PEDOT:PSS) is a widely used HTL material because it is easily deposited by spin-coating and shows the high work function (Φ) of ~ 5.2 eV, which is well matched to the highest occupied molecular orbital (HOMO) level of many of the polymers used as active layers [19,20]. However, the acidity and water-absorbing tendency of PEDOT:PSS cause poor device performance and stability [21].

Solution-processed metal oxides such as molybdenum oxide (MoO_x) [22,23], tungsten oxide (WO_x) [11,24], vanadium oxide (VO_x) [25], copper oxide (CuOx) [26] and nickel oxide (NiO_x) [27] have emerged as alternative HTL materials for PSCs because they show excellent stability and Φ values that match those of active layer materials. Among them, NiO_x has a HOMO level well-aligned to those of many polymers, as well as showing excellent stability [28]. In addition, nickel acetate tetrahydrate and monoethanolamine (MEA) precursors for NiO_x can be spin-coated to form NiO_x thin films after a simple annealing process, demonstrating solution-processable NiO_x (s-NiO_x) fabrication. In this work, we report the use of highly stable and solution processable s-NiO_x as HTL material and investigate the structural, morphological, and optical properties of s-NiO_x thin films. A PSC based on a BHJ of random-polymer RP(BDT-

PDBT) [29] and $PC_{70}BM$ using s-NiO_x as an HTL exhibits improved stability and efficiency compared to a conventional device utilizing PEDOT:PSS as the HTL.

Fig. 1 shows the ultraviolet–visible–near-infrared (UV-Vis-NIR) absorption and transmission spectra of the s-NiO_x thin films post-annealed at 300, 400, and 500 °C on a simple hot plate. In the s-NiO_x layer annealed at 300 °C, the precursor is completely converted into NiO_x, as indicated by the strong band-edge absorption peak at 350 nm. NiO_x exhibits clear absorption onset at ~370 nm regardless of the annealing temperature, indicating an optical band gap of ~3.3 eV. This is in good agreement with previously reported values [30-32]. The transmission spectra of the post-annealed s-NiO_x film show high transparencies, which are suitable for application as window layers in PSCs.

To understand the chemical and electronic states of the s-NiO_x film post-annealed at 500 °C, the film was analyzed by X-ray photoelectron spectroscopy (XPS). Fig. 2a shows the XPS spectrum for the Ni $2p_{3/2}$ level, which is deconvoluted into three peaks (see supporting information Fig. S1 for the XPS spectra of s-NiO_x films post-annealed at various temperatures). The peak at 853.7 eV corresponds to Ni^{2+} species in the standard Ni–O octahedral bonding configuration in cubic rock-salt NiO [33-35]. The second broad peak centered at 855.6 eV is ascribed to the Ni^{2+} vacancy-induced Ni^{3+} ion [33,34,36]. The third broad peak centered at 861.8 eV is also assigned to the NiO structure [33,34,36]. Fig. 2b shows the XPS spectrum for the O 1*s* energy level, which is deconvoluted into two distinct peaks. The peak centered at 528.9 eV confirms the occurrence of Ni−O octahedral bonding in NiO. The peak at 532.2 eV indicates the presence of both NiO and Ni_2O_3 [30,35].

To investigate the post-annealing temperature effects on the surface properties of s-NiO_x thin films, the film morphologies were examined using atomic force microscopy (AFM). The

nickel ink precursor was spin-coated onto indium tin oxide (ITO) substrates and post-annealed at 300, 400, and 500 °C on a simple hot plate in air for 1 h. The topography and phase imaging of the s-NiO_x films are shown in Fig. 3. The s-NiO_x films post-annealed at 300 °C and 400 °C show larger triangular grains with root-mean-square (RMS) roughness values of 2.4 and 1.2 nm, respectively. The s-NiO_x film post-annealed at 500 °C shows uniformly shaped grains with the RMS value of 0.8 nm. This result indicates that the post-annealing temperature influences surface roughness and morphology of the s-NiO_x film. However, the RMS values of the films post-annealed at 300 °C and 400 °C are higher than that of the film post-annealed at 500 °C. The RMS value therefore depends on both the preparation and the post-annealing temperature.

s-NiO_x as the HTL and RP(BDT-PDBT):$PC_{70}BM$ photoactive layers were used to fabricate photovoltaic cells. The device structure and the energy band diagram of the s-NiO_x device are shown in Fig. 4, along with those of the reference PEDOT:PSS devices. The energy level of RP(BDT-PDBT) is determined using electrochemical cyclic voltammetry. The energy levels of s-NiO_x are determined using ultraviolet photoelectron spectroscopy (UPS) and UV-Vis-NIR spectroscopy. The energy levels of ITO, PEDOT:PSS, $PC_{70}BM$, and aluminium (Al) are taken from previously reported results [37-40]. All device fabrication details are reported in the experimental section. We fabricated PSCs with different post-annealed s-NiO_x films as HTLs. The current density–voltage (J–V) characteristics and incident photon-to-current efficiency (IPCE) of the solar cells are presented in Fig. 5; the characteristics of their performances are summarized in Table 1. At processing temperatures of 300 °C and 400 °C, the precursor decomposes into s-NiO_x and develops a high RMS roughness value, showing poor PSC performance compared to the film post-annealed at 500 °C. The best-performing PSC has a PCE of 4.46%, short-circuit current density (J_{sc}) of 9.85 mA/cm^2, open-circuit voltage (V_{oc}) of 0.71, and fill factor (FF) of 63% and uses an HTL of s-NiO_x film (RMS = 0.8 nm). However, the PSC

using an s-NiO_x film with an RMS of 2.4 nm as the HTL shows the lowest PCE of 3.72%, with the J_{sc} decreased to 8.71 mA/cm^2.

The effective interfacial area between the s-NiO_x and the active layer depends on the surface roughness of s-NiO_x. The RMS value of 0.8 nm corresponds to the smallest effective surface area; the film with this RMS value forms the smallest effective interfacial area, whereas the film post-annealed at 300 °C has the largest. For comparison of the performance of solar cells with our s-NiO_x HTL, we fabricated PEDOT:PSS-based devices and operated the cells side-by-side. The optimized PEDOT:PSS-based device showed a PCE of 4.05%, while the optimized s-NiO_x devices showed a PCE of 4.46%

During this study, significantly enhanced stability was observed in the s-NiO_x devices compared to that of the conventional PEDOT:PSS-based devices. Stability measurements were performed on un-encapsulated s-NiO_x and PEDOT:PSS-based devices stored at ambient conditions for 300 min. As shown in Fig. 6, the s-NiO_x-based device degrades much more slowly than the PEDOT:PSS-based devices. The performance of the conventional device degrades by the loss of J_{sc}, attributed to the degradation of the HTL and/or the interface because of the acidic and hygroscopic nature of PEDOT:PSS, which corrodes the ITO electrode [41-43].

In conclusion, we newly synthesized solution-processable s-NiO_x for use as an efficient HTL material and investigated the morphological and optical properties of the s-NiO_x film. PSCs with RP(BDT-PDBT) and $PC_{70}BM$ active layers and s-NiO_x as HTL exhibited significant enhancements in FF and PCE compared to conventional PEDOT:PSS-based solar cells. The post-annealing temperature and the surface roughness both affected the solar cell performance. Importantly, the s-NiO_x device exhibited significantly enhanced stability compared to the

conventional device with the PEDOT:PSS HTL. Therefore, we believe that s-NiO_x could be an alternative functional interface material in solution-processable optoelectronic devices.

Experimental Section

NiOx precursor synthesis

A 285mg of nickel acetate tetrahydrate (Ni(CH3COO)2.4H2O) was dissolved in a 10 ml of ethanol with a 61 mg of monoethanolamine (NH2CH2CH2OH). The mole ratio of Ni(CH3COO)2.4H2O:NH2CH2CH2OH was maintained at 1:1 in ethanol solution. The prepared solution was stirred at 70 °C for 3 hours in a sealed glass vial to obtain homogeneous and deep green colour solution. The prepared solution was used within a month without segregation.

HTL thin-film deposition and characterization

PEDOT:PSS (Baytron PH) aqueous solution was spin-cast at 4500 rpm, and 40 sec on UV-Ozone treated ITO substrates. The PEDOT:PSS coated substrate was baked at 140 °C for 10 min in atmospheric conditions. The NiO_x precursor solution was spin-coated at a rotation speed of 7000 rpm and 40 sec on the pre UV-Ozone (10 min) treated ITO substrates. The NiOx coated substrates were baked at 120 °C for 10 min then the substrates were post annealed at 300°C, 400°C and 500 °C, respectively for 1 hour. The thickness of the as-prepared s-NiOx film was ~30 nm, but decreased to ~18 nm after the post-annealing process.

Device Fabrication and Characterization

The PEDOT:PSS and s-NiOx (~18 nm) HTL coated ITO substrates were transferred to the nitrogen (N_2) filled glove box for active layer deposition. A 10mg of RP(BDT-PDBT) and 15mg of $PC_{70}BM$ was dissolved in 3 vol% of diphenylether as an additive then a 1 ml of dichlorobenzene was added. The detailed synthesis and characterization of RP(BDT-PDBT) are presented in previous report [29] with supporting information. The prepared polymer blended mixture solution was stirred at a speed of 450 rpm and maintained at 40 °C in the N_2 glove box over 12 hour. The active layer was deposited by spin coating RP(BDT-PDBT:$PC_{70}BM$ blended solution) at 1000 rpm and 70 sec on HTL coated ITO substrates. The active layer (~75 nm) deposited on HTL/ITO substrate was maintained at room temperature for 30 minute in the nitrogen (N_2) filled glove box for evaporation of excess solvent from the active layer. Subsequently, Al (~100 nm) electrodes were deposited using shadow mask via thermal evaporation in a vacuum ($<5 \times 10^{-4}$ Pa). The active area of device was about 0.038 cm^2.

Characterization

The crystalline structure was confirmed by X-ray diffraction (XRD) (Rigahu-Smart Lab). s-NiOx thin-films was analyzed using XPS (Thermo Scientific) measurements. Optical transmittance and absorption spectra of s-NiOx thin-films were measured using a JASCO V-570 double-beam spectrophotometer in the wavelength ranging between 200-2500 nm, with quartz substrate in the reference path of the beam. Hence, the shown transmittance spectra do not include the effect of quartz substrate. The surface microstructure was analyzed by an Asylum MFP 3D atomic force microscope (AFM) operated in AC mode. The current-voltage (J–V) characteristics were recorded using a Keithley 2400 Source Meter in the 100 mW/cm^2 simulated AM of 1.5 G irradiation (Science tech SS-0.5K Solar Simulator). The light intensity was measured by using a photometer (International light, IL1400) and corrected using a standard silicon solar cell. All the measurements were performed under ambient atmospheric conditions at room temperature.

Acknowledgment

This work was supported by a Research Grant of Pukyong National University (2016 year)

References

[1] J.Y. Kim, K. Lee, N.E. Coates, D. Moses, T.-Q. Nguyen, M. Dante, A.J. Heeger, Efficient tandem polymer solar cells fabricated by all-solution processing., Science 317 (2007) 222–5.

[2] S.H. Park, A. Roy, S. Beaupré, S. Cho, N. Coates, J.S. Moon, D. Moses, M. Leclerc, K. Lee, A.J. Heeger, Bulk heterojunction solar cells with internal quantum efficiency approaching 100%, Nat. Photonics. 3 (2009) 297–302.

[3] F.C. Krebs, T. Tromholt, M. Jørgensen, Upscaling of polymer solar cell fabrication using full roll-to-roll processing, Nanoscale. 2 (2010) 873.

[4] G. Li, R. Zhu, Y. Yang, Polymer solar cells, Nat. Photonics. 6 (2012) 153–161.

[5] A.J. Heeger, 25th anniversary article: Bulk heterojunction solar cells: Understanding the mechanism of operation, Adv. Mater. 26 (2014) 10–28.

[6] H. Zhou, L. Yang, A.C. Stuart, S.C. Price, S. Liu, W. You, Development of Fluorinated Benzothiadiazole as a Structural Unit for a Polymer Solar Cell of 7 % Efficiency, Angew. Chemie Int. Ed. 50 (2011) 2995–2998.

[7] W. Zhao, D. Qian, S. Zhang, S. Li, O. Inganäs, F. Gao, J. Hou, Fullerene-Free Polymer Solar Cells with over 11% Efficiency and Excellent Thermal Stability, Adv. Mater. 28 (2016) 4734–4739.

[8] H. Bin, L. Gao, Z.-G. Zhang, Y. Yang, Y. Zhang, C. Zhang, S. Chen, L. Xue, C. Yang, M. Xiao, Y. Li, 11.4% Efficiency non-fullerene polymer solar cells with trialkylsilyl substituted 2D-conjugated polymer as donor, Nat. Commun. 7 (2016) 13651.

[9] J.Y. Kim, S.H. Kim, H.-H. Lee, K. Lee, W. Ma, X. Gong, A.J. Heeger, New Architecture for High-Efficiency Polymer Photovoltaic Cells Using Solution-Based Titanium Oxide as an Optical Spacer, Adv. Mater. 18 (2006) 572–576.

[10] A. Roy, S.H. Park, S. Cowan, M.H. Tong, S. Cho, K. Lee, A.J. Heeger, Titanium suboxide as an optical spacer in polymer solar cells, Appl. Phys. Lett. 95 (2009) 13302.

[11] F. Guillain, D. Tsikritzis, G. Skoulatakis, S. Kennou, G. Wantz, L. Vignau, Annealing-free solution-processed tungsten oxide for inverted organic solar cells, Sol. Energy Mater. Sol. Cells. 122 (2014) 251–256.

[12] Z. Zheng, S. Zhang, J. Zhang, Y. Qin, W. Li, R. Yu, Z. Wei, J. Hou, Over 11% Efficiency in Tandem Polymer Solar Cells Featured by a Low-Band-Gap Polymer with Fine-Tuned Properties, Adv. Mater. 28 (2016) 5133–5138.

[13] L. Lu, T. Xu, W. Chen, E.S. Landry, L. Yu, Ternary blend polymer solar cells with enhanced power conversion efficiency, Nat. Photonics. 8 (2014) 716–722.

[14] S.H. Park, I. Shin, K.H. Kim, R. Street, A. Roy, A.J. Heeger, Tandem Solar Cells Made from Amorphous Silicon and Polymer Bulk Heterojunction Sub-Cells, Adv. Mater. 27 (2015) 298–302.

[15] M.D. Irwin, D.B. Buchholz, A.W. Hains, R.P.H. Chang, T.J. Marks, p-Type semiconducting nickel oxide as an efficiency-enhancing anode interfacial layer in polymer bulk-heterojunction solar cells, Proc. Natl. Acad. Sci. 105 (2008) 2783–2787.

[16] S.-S. Li, K.-H. Tu, C.-C. Lin, C.-W. Chen, M. Chhowalla, Solution-Processable Graphene Oxide as an Efficient Hole Transport Layer in Polymer Solar Cells, ACS Nano. 4 (2010) 3169–3174.

[17] M. Jørgensen, K. Norrman, S.A. Gevorgyan, T. Tromholt, B. Andreasen, F.C. Krebs, Stability of Polymer Solar Cells, Adv. Mater. 24 (2012) 580–612.

[18] H. Pan, L. Zuo, W. Fu, C. Fan, B. Andreasen, X. Jiang, K. Norrman, F.C. Krebs, H. Chen, MoO3–Au composite interfacial layer for high efficiency and air-stable organic solar cells, Org. Electron. 14 (2013) 797–803.

[19] S.A. Carter, M. Angelopoulos, S. Karg, P.J. Brock, J.C. Scott, Polymeric anodes for improved polymer light-emitting diode performance, Appl. Phys. Lett. 70 (1997) 2067–2069.

[20] L. Groenendaal, F. Jonas, D. Freitag, H. Pielartzik, J.R. Reynolds, Poly(3,4-ethylenedioxythiophene) and Its Derivatives: Past, Present, and Future, Adv. Mater. 12 (2000) 481–494.

[21] Y. Suh, N. Lu, S.H. Lee, W.-S. Chung, K. Kim, B. Kim, M.J. Ko, M.J. Kim, Degradation of a Thin Ag Layer Induced by Poly(3,4-ethylenedioxythiophene):Polystyrene Sulfonate in a Transmission Electron Microscopy Specimen of an Inverted Polymer Solar Cell, ACS Appl. Mater. Interfaces. 4 (2012) 5118–5124.

[22] Y. Sun, C.J. Takacs, S.R. Cowan, J.H. Seo, X. Gong, A. Roy, A.J. Heeger, Efficient, Air-Stable Bulk Heterojunction Polymer Solar Cells Using MoOx as the Anode Interfacial Layer, Adv. Mater. 23 (2011) 2226–2230.

[23] N.K. Elumalai, A. Saha, C. Vijila, R. Jose, Z. Jie, S. Ramakrishna, Enhancing the stability of polymer solar cells by improving the conductivity of the nanostructured MoO3 hole-transport layer, Phys. Chem. Chem. Phys. 15 (2013) 6831.

[24] Z. Tan, L. Li, C. Cui, Y. Ding, Q. Xu, S. Li, D. Qian, Y. Li, Solution-Processed Tungsten Oxide as an Effective Anode Buffer Layer for High-Performance Polymer Solar Cells, J. Phys. Chem. C. 116 (2012) 18626–18632. doi:10.1021/jp304878u.

[25] J.-S. Huang, C.-Y. Chou, M.-Y. Liu, K.-H. Tsai, W.-H. Lin, C.-F. Lin, Solution-processed vanadium oxide as an anode interlayer for inverted polymer solar cells hybridized with ZnO nanorods, Org. Electron. 10 (2009) 1060–1065.

[26] Q. Xu, F. Wang, Z. Tan, L. Li, S. Li, X. Hou, G. Sun, X. Tu, J. Hou, Y. Li, High-Performance Polymer Solar Cells with Solution-Processed and Environmentally Friendly CuOx Anode Buffer Layer, ACS Appl. Mater. Interfaces, 5 (2013) 10658-10664.

[27] X. Fan, G. Fang, F. Cheng, P. Qin, H. Huang, Y. Li, Enhanced performance and stability in PBDTTT-C-T : PC 70 BM polymer solar cells by optimizing thickness of NiO x buffer layers, J. Phys. D. Appl. Phys. 46 (2013) 305106.

[28] S. Bai, M. Cao, Y. Jin, X. Dai, X. Liang, Z. Ye, M. Li, J. Cheng, X. Xiao, Z. Wu, Z. Xia, B. Sun, E. Wang, Y. Mo, F. Gao, F. Zhang, Low-Temperature Combustion-Synthesized Nickel Oxide Thin Films as Hole-Transport Interlayers for Solution-Processed Optoelectronic Devices, Adv. Energy Mater. 4 (2014) 1301460.

[29] M.H. Tamilavan, V.; Kim, S.; Agneeswari, R.; Lee, D.; Cho, S.; Jin, Y.; Jeong, J.; Park, S. H.; Hyun, Efficient Ternary Copolymers Incorporating Electron Rich Benzodithiophene and Electron Accepting Pyrrolo[3,4-c]pyrrole-1,3-dione and Difluorobenzothiadiazole derivatives for polymer solar cells, Polym. Bull. (***Revision Submitted***).

[30] J.R. Manders, S.-W. Tsang, M.J. Hartel, T.-H. Lai, S. Chen, C.M. Amb, J.R. Reynolds, F. So, Solution-Processed Nickel Oxide Hole Transport Layers in High Efficiency Polymer Photovoltaic Cells, Adv. Funct. Mater. 23 (2013) 2993–3001.

[31] J.-Y. Jeng, K.-C. Chen, T.-Y. Chiang, P.-Y. Lin, T.-D. Tsai, Y.-C. Chang, T.-F. Guo, P. Chen, T.-C. Wen, Y.-J. Hsu, Nickel Oxide Electrode Interlayer in CH 3 NH 3 PbI 3 Perovskite/PCBM Planar-Heterojunction Hybrid Solar Cells, Adv. Mater. 26 (2014) 4107–4113.

[32] S. Liu, R. Liu, Y. Chen, S. Ho, J.H. Kim, F. So, Nickel Oxide Hole Injection/Transport Layers for Efficient Solution-Processed Organic Light-Emitting Diodes, Chem. Mater. 26 (2014) 4528–4534.

[33] K.S. Kim, N. Winograd, X-ray photoelectron spectroscopic studies of nickel-oxygen surfaces using oxygen and argon ion-bombardment, Surf. Sci. 43 (1974) 625–643.

[34] S. Uhlenbrock, C. Scharfschwerdt, M. Neumann, G. Illing, H.-J. Freund, The influence of defects on the Ni 2p and O 1s XPS of NiO, J. Phys. Condens. Matter. 4 (1992) 7973–7978.

[35] B. Sasi, K.G. Gopchandran, Nanostructured mesoporous nickel oxide thin films, Nanotechnology. 18 (2007) 115613.

[36] M. Tomellini, X-ray photoelectron spectra of defective nickel oxide, J. Chem. Soc. Faraday Trans. 1 Phys. Chem. Condens. Phases. 84 (1988) 3501.

[37] Z. Ma, Z. Tang, E. Wang, M.R. Andersson, O. Inganäs, F. Zhang, Influences of Surface Roughness of ZnO Electron Transport Layer on the Photovoltaic Performance of Organic Inverted Solar Cells, J. Phys. Chem. C. 116 (2012) 24462–24468.

[38] K.X. Steirer, P.F. Ndione, N.E. Widjonarko, M.T. Lloyd, J. Meyer, E.L. Ratcliff, A. Kahn, N.R. Armstrong, C.J. Curtis, D.S. Ginley, J.J. Berry, D.C. Olson, Enhanced Efficiency in Plastic Solar Cells via Energy Matched Solution Processed NiOx Interlayers, Adv. Energy Mater. 1 (2011) 813–820.

[39] R. Betancur, M. Maymó, X. Elias, L.T. Vuong, J. Martorell, Sputtered NiO as electron blocking layer in P3HT:PCBM solar cells fabricated in ambient air, Sol. Energy Mater. Sol. Cells. 95 (2011) 735–739.

[40] E.L. Ratcliff, J. Meyer, K.X. Steirer, A. Garcia, J.J. Berry, D.S. Ginley, D.C. Olson, A. Kahn, N.R. Armstrong, Evidence for near-Surface NiOOH Species in Solution-Processed NiO x Selective Interlayer Materials: Impact on Energetics and the Performance of Polymer Bulk Heterojunction Photovoltaics, Chem. Mater. 23 (2011) 4988–5000.

[41] X. Bulliard, S.-G. Ihn, S. Yun, Y. Kim, D. Choi, J.-Y. Choi, M. Kim, M. Sim, J.-H. Park, W. Choi, K. Cho, Enhanced Performance in Polymer Solar Cells by Surface Energy Control, Adv. Funct. Mater. 20 (2010) 4381–4387.

[42] Y. Sun, J.H. Seo, C.J. Takacs, J. Seifter, A.J. Heeger, Inverted Polymer Solar Cells Integrated with a Low-Temperature-Annealed Sol-Gel-Derived ZnO Film as an Electron Transport Layer, Adv. Mater. 23 (2011) 1679–1683.

[43] Z. Tang, L.M. Andersson, Z. George, K. Vandewal, K. Tvingstedt, P. Heriksson, R. Kroon, M.R. Andersson, O. Inganäs, Interlayer for Modified Cathode in Highly Efficient Inverted ITO-Free Organic Solar Cells, Adv. Mater. 24 (2012) 554–558.

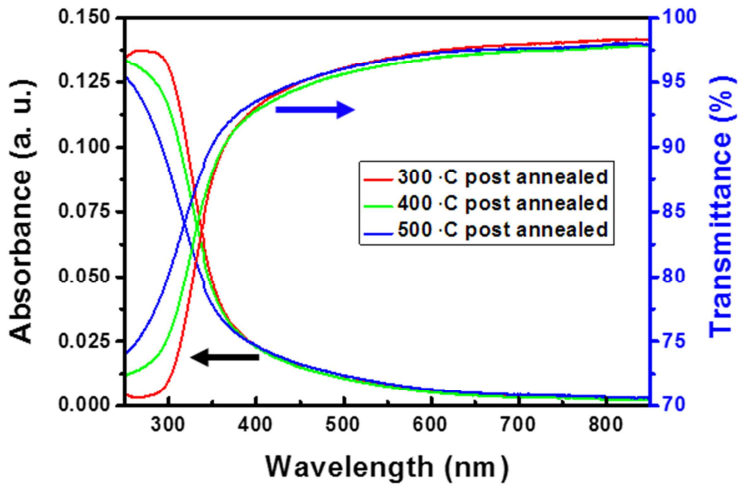

Fig. 1 Transmittance and absorbance spectra of the s-NiO_x films prepared on quartz substrates.

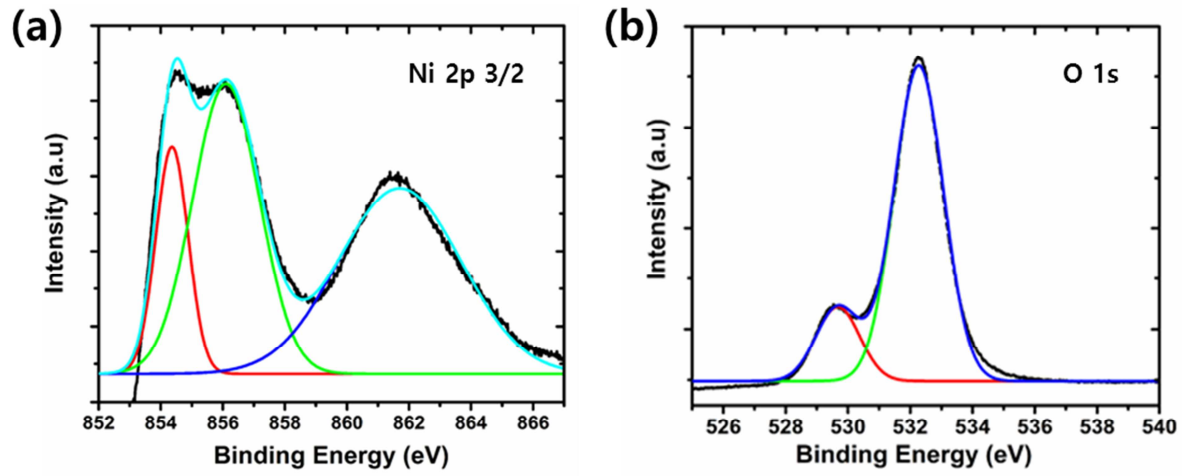

Fig. 2 The (a) Ni $2p_{3/2}$ and (b) O 1*s* orbitals of s-NiO_x post-annealed at 500 °C.

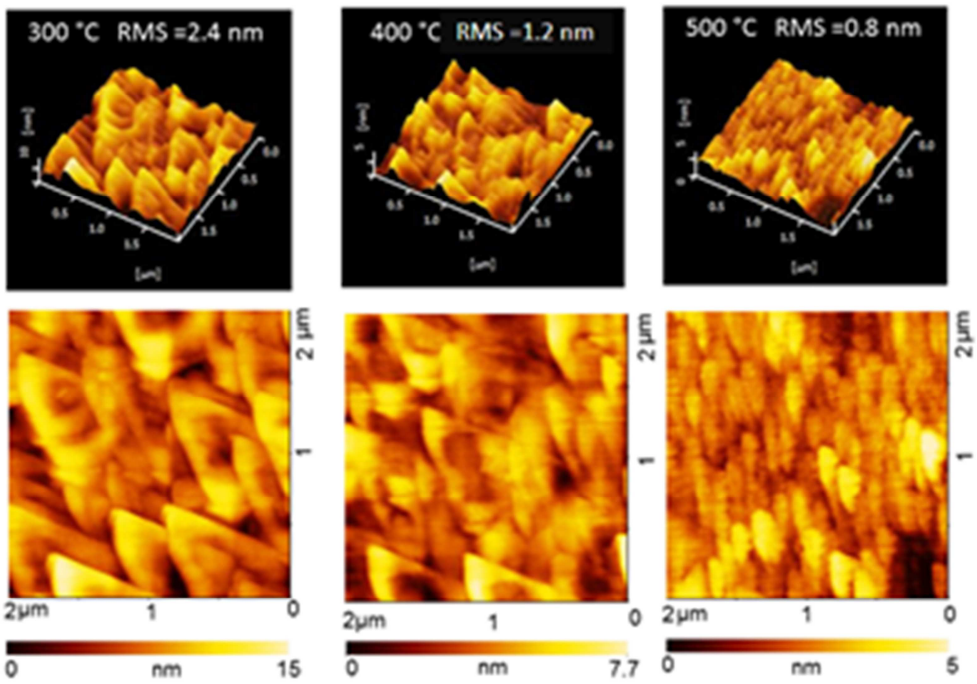

Fig. 3 AFM images of the s-NiO_x thin films at various post-annealing temperatures.

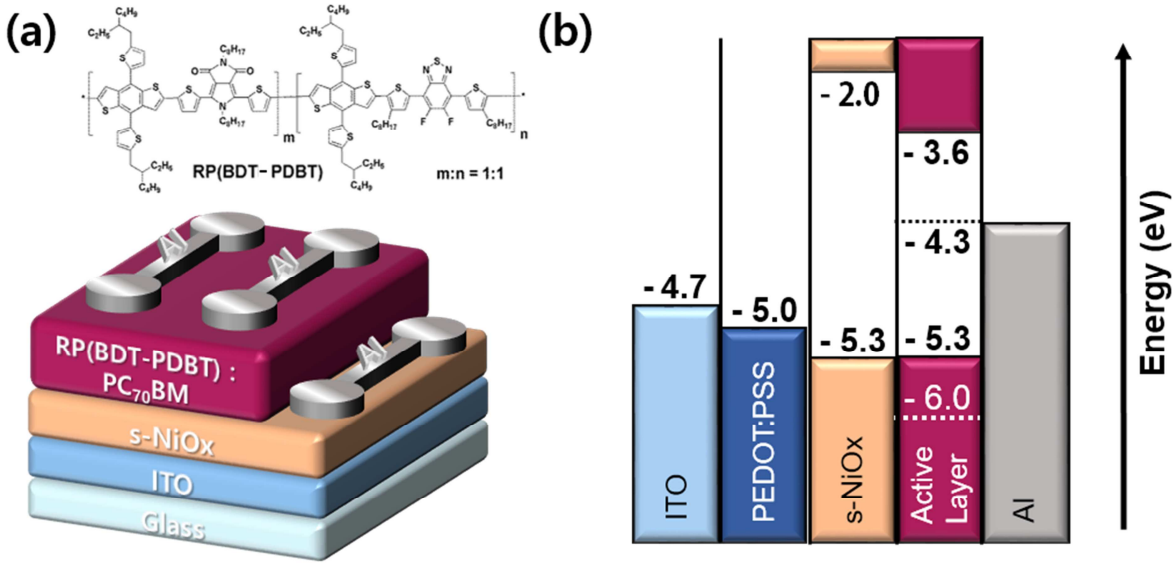

Fig. 4 (a) Device structure of the PSCs and (b) schematic energy diagram of the polymer, TCO, HTL, and Al electrode.

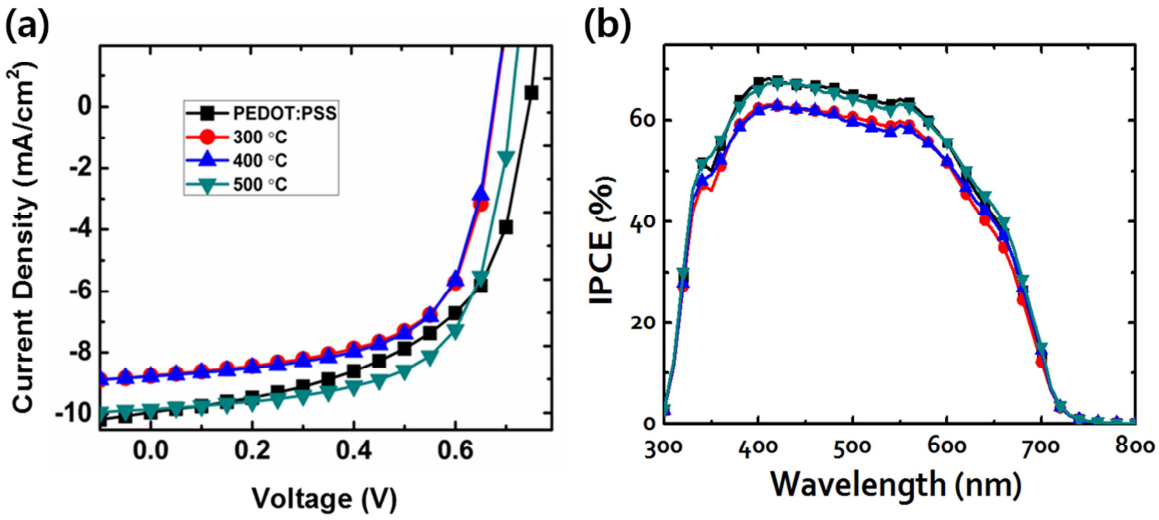

Fig. 5 (a) J–V curves of the PSCs under the illumination of AM 1.5G, 100 mW/cm^2 and (b) IPCE spectra of the PSCs,

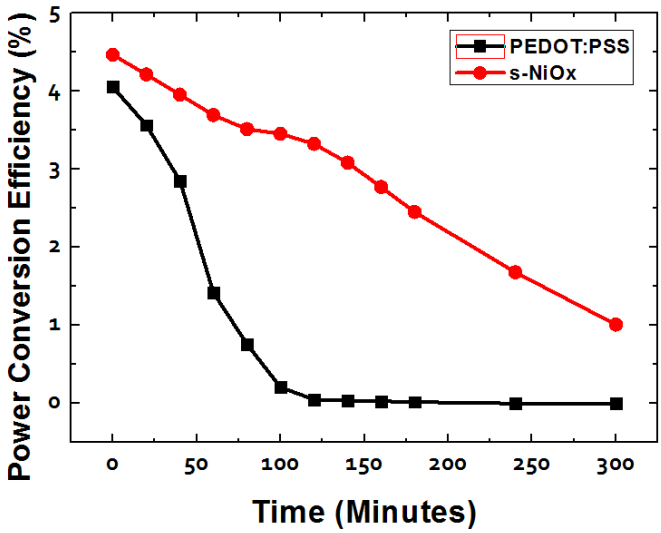

Fig. 6 Stability of PSCs using s-NiO_x and PEDOT:PSS as HTLs as a function of time.

Table 1. Device characteristics of the solar cells.

Hole Transport Layer	J_{sc} (mA/cm^2)	V_{oc} (mV)	FF (%)	PCE (%)
PEDOT:PSS	9.94	0.74	54.5	4.05 ± 0.03 [a]
PEDOT:PSS, Stability after 1 h	2.91	0.72	53.0	1.12 ± 0.02
PEDOT:PSS, Stability after 2 h	0.21	0.21	21.2	0.05 ± 0.01
s-NiO_x, 300 °C	8.71	0.68	61.0	3.69 ± 0.03
s-NiO_x, 400 °C	8.78	0.68	62.0	3.75 ± 0.02
s-NiO_x, 500 °C	9.85	0.71	63.0	4.45 ± 0.01
s-NiO_x, 500 °C, Stability after 1 h	8.38	0.70	62.6	3.69 ± 0.03
s-NiO_x, 500 °C, Stability after 2 h	7.83	0.69	61.5	3.35 ± 0.01

[a] The average values of the PCEs based on twenty devices are prepared in parentheses.

Research Highlight

- Solution-processed nickel oxide (s-NiO_x) was synthesized for use as hole-transport layers (HTLs) in the fabrication of polymer solar cell (PSC) devices.

- The nickel acetate precursor fully decomposes and forms s-NiO_x films, which shows larger crystalline grain sizes with lower root mean square roughness.

- The PSC fabricated using s-NiO_x as HTLs exhibit the enhanced efficiency of 4.46% and better stability compared to conventional PSCs using poly (3,4-ethylenedioxythiophene):poly(styrene sulfonate) as HTLs.